Diverse Deformation Patterns of Aleutian Volcanoes From Satellite Interferometric Synthetic Aperture Radar (InSAR)

Zhong Lu[1], Daniel Dzurisin[2], Charles Wicks, Jr.[3], John Power[4], Ohig Kwoun[5], and Russell Rykhus[5]

Interferometric synthetic aperture radar (InSAR) is capable of measuring ground-surface deformation with centimeter-to-subcentimeter precision at a spatial resolution of tens of meters over a large region. With its global coverage and all-weather imaging capability, InSAR has become an increasingly important measurement technique for constraining magma dynamics of volcanoes over remote regions such as the Aleutian Islands. The spatial distribution of surface deformation data derived from InSAR images enables the construction of detailed mechanical models to enhance the study of magmatic processes. This paper summarizes the diverse deformation patterns of the Aleutian volcanoes observed with InSAR. These include the following: 1) inflation of Mount Peulik Volcano preceding a seismic swarm at nearby Becharof Lake in 1998; 2) persistent volcano-wide subsidence at Aniakchak and Fisher Volcanoes; 3) magmatic intrusion and associated tectonic stress release at Akutan Volcano; 4) magmatic intrusion at Makushin Volcano associated with a small eruption in 1995; 5) complex patterns of transient deformation during and after the 1992–93 eruption at Seguam Volcano; 6) subsidence caused by a decrease in pore fluid pressure in an active hydrothermal system beneath Kiska Volcano; and 7) lack of expected deformation associated with recent eruptions at Shishaldin, Pavlof, Cleveland, and Korovin Volcanoes. We also present preliminary InSAR results for the Katmai Volcano group, and Chiginagak and Dutton Volcanoes. These studies demonstrate that deformation patterns and associated magma supply mechanisms in the Aleutians are diverse and vary between volcanoes. These findings provide an improved understanding of magmatic plumbing systems in the Aleutians.

[1] U.S. Geological Survey (USGS), Earth Resources Observation & Science (EROS) Center and Cascades Volcano Observatory, Vancouver, Washington, USA; lu@usgs.gov

[2] USGS, Cascades Volcano Observatory, Vancouver, Washington, USA; dzurisin@usgs.gov

[3] USGS, Earthquake & Volcano Hazards Programs, Menlo Park, California, USA; cwicks@usgs.gov

[4] USGS, Alaska Volcano Observatory, Anchorage, Alaska, USA; jpower@usgs.gov

[5] SAIC, contractor to the USGS EROS Center, Sioux Falls, South Dakota, USA; okwoun@usgs.gov, rykhus@usgs.gov

Volcanism and Subduction: The Kamchatka Region
Geophysical Monograph Series 172

10.1029/172GM18

1. INTRODUCTION

The general eruption cycle of a volcano can be conceptualized as a series of events from deep magma generation to surface eruption, including such stages as partial melting, initial ascent through the upper mantle and lower crust, crustal assimilation, magma mixing, degassing, shallow storage, and finally, ascent to the surface [Dzurisin, 2003]. This process is complex, varying from one eruption to the next and from volcano to volcano. However, in many cases, volcanic eruptions are preceded by pronounced ground deformation in response to increasing pressure in magma reservoirs or upward intrusion of magma [Dvorak and Dzurisin, 1997]. Magma reser-

voirs typically occur at or below the brittle-ductile transition in the crust (~5 km beneath volcanoes). Even though the slow ascent of magma to that depth generally is not marked by earthquakes [e.g., Sibson, 1982], magma accumulation causes surface deformation. This deformation can be subtle—especially if intrusion occurs episodically in a series of small events or gradually over a long time period. Therefore, surface deformation patterns can provide important insight into the structure, plumbing, and state of restless volcanoes [Dvorak and Dzurisin, 1997; Dzurisin, 2003 and 2007]. Deformation can be the first sign of increasing levels of magmatic activity, preceding increased seismicity or other precursors that signal impending intrusions or eruptions.

The Aleutian arc contains about 8 percent of the world's active volcanoes and more than 85 percent of the nation's historically active volcanoes. During the past decade, there has been an average of 3–4 explosive eruptions per year in the arc. Aleutian volcanoes span the entire spectrum in eruptive style, size, volume, and magma composition. Although the rate of eruptive activity is very high, deformation monitoring using the Global Positioning System (GPS) has been possible at only a few Aleutian volcanoes, owing to the remote location, hostile climate, difficult logistics, and high cost of field operations.

Interferometric synthetic aperture radar (InSAR) imaging is a recently developed remote sensing technique involving the use of two or more synthetic aperture radar (SAR) images to image surface topography and subtle changes due to deformation [e.g., Massonnet & Feigl, 1998; Zebker et al., 2000]. InSAR combines phase information from two or more SAR images of the same area acquired from similar vantage points at different times to produce an interferogram. The interferogram, depicting range changes between the radar and the ground, can be further processed with a digital elevation model (2-pass InSAR) to image surface deformation at a horizontal resolution of tens of meters over areas of ~100 km by 100 km with centimeter-to-subcentimeter precision under favorable conditions. Because SAR operates at a microwave wavelength (from a few millimeters to tens of centimeters), it can penetrate clouds and rain during the day and at night. Therefore, all-weather satellite InSAR images with the potential for measuring subtle ground surface deformation are useful for studying the magma plumbing systems of Aleutian volcanoes. SAR satellites that can provide InSAR capability for deformation mapping are described in Table 1.

To better understand magmatic processes, numerical models are often employed to invert the InSAR-derived surface deformation for physical parameters of a magma body. The spatial resolution of surface displacement data provided by InSAR makes it possible to constrain models of volcanic deformation with a variety of source geometries, such as the spherical point pressure source (Mogi source) [Mogi, 1958], the dislocation source (sill or dike source) [Okada, 1985], the ellipsoid source [Davis, 1986; Yang et al., 1988], the penny-shaped crack source [Fialko et al., 2001], etc. The most widely used source in volcano deformation modeling is the point source embedded in elastic homogeneous half-space [Mogi, 1958]. Even though the point source is simplest, it can fit observed deformation data remarkably well. The four parameters used to describe the point source are horizontal location coordinates (x, y), depth, and pressure or volume change. Another frequently used model is the rectangular elastic dislocation source [Okada, 1985], which requires eight model parameters: horizontal location coordinates, depth, length, width, strike and dip of the dislocation surface, and the slip directed perpendicular to the dislocation surface (i.e., expansion or contraction). Nonlinear least-squares inversion techniques are often used to optimize the source parameters [e.g., Cervelli et al., 2001]. Multiple InSAR images allow evaluation of the temporal progression of a deformation source and the associated magmatic process.

2. INSAR-BASED DEFORMATION SURVEY OF ALEUTIAN VOLCANOES

2.1. Augustine Volcano

Augustine Volcano (Plate 1a), an 8-by-11-km island stratovolcano in Cook Inlet, erupted in 1935, 1963–64, 1976, 1986, and January–March 2006, each time producing andesitic pyroclastic flows and lava domes from vents in the summit area. Multiple InSAR images constructed from SAR images acquired from 1992 to 2004 by the European Remote Sensing Satellite (ERS)-1 and ERS-2 (Table 1) show no sign of significant volcano-wide deformation. Throughout that period, a sector of the volcano's north flank mantled by 1976 and 1986 pyroclastic flows experienced subsidence/compaction at a rate of about 3 cm per year (Plate 1a). The observed deformation can be used to study physical characteristics of the 1986 flows [Masterlark et al., 2006].

2.2. Katmai Volcano Group

The Katmai group (Plate 1b) consists of five volcanoes: Martin, Mageik, Trident, Novarupta, and Katmai. In 1912, Katmai was the site of the world's largest volcanic eruption of the 20th century. The eruption produced ~20 km^3 of air-fall tephra, 11–15 km^3 of ash-flow tuff, and the Novarupta lava dome in the Valley of Ten Thousand Smokes [Miller et al., 1998; Hildreth, 1983]. Eruptive activity in the Katmai group since 1912 has included lava flows from the New Trident vent on Trident Volcano, the youngest of which erupted in 1963. The first application of InSAR to study surface deformation

Table 1. Spaceborne SAR sensors capable of deformation mapping

Mission	Agency	Period of Operation[1]	Orbit Repeat Cycle	Frequency	Wave-length	Incidence Angle at Swath Center	Resolution
Seasat	NASA[2]	06/27 to 10/10, 1978	17 days	L-band 1.2 GHz	25 cm	20 to 26 degrees	25 m
ERS-1	ESA[3]	07/1991 to 03/2000	3, 168, and 35 days[4]	C-band 5.3 GHz	5.66 cm	23 degrees	30 m
SIR-C/X-SAR	NASA, DLR[5], and ASI[6]	04/09 to 04/20, 1994, and 09/30 to 10/11, 1994	6-month, 1-, 2-, 3-day[7]	L-band 1.249 GHz C-band 5.298 GHz X-band 9.6 GHz	24.0 cm 5.66 cm 3.1 cm	17 to 63 degrees (L- & C-band) 54 degrees (X-band)	10–200 m (30 m typical)
JERS-1	JAXA[8]	02/1992 to 10/1998	44 days	L-band 1.275 GHz	23.5 cm	39 degrees	20 m
ERS-2	ESA	04/1995 to present	35 days	5.3 GHz	5.66 cm	23 degrees	30 m
Radarsat-1	CSA[9]	11/1995 to present	24 days	C-band 5.3 GHz	5.66 cm	10 to 60 degrees	10–100 m
Envisat	ESA	03/2002 to present	35 days	C-band 5.331 GHz	5.63 cm	15 to 45 degrees	20–100 m
ALOS	JAXA	Jan 2006 to present	46 days	L-band 1.270 GHz	23.6 cm	8 to 60 degrees	10–100 m

[1] Information was current in January 2006.
[2] National Aeronautics and Space Agency
[3] European Space Agency
[4] To accomplish various mission objectives, the ERS-1 repeat cycle was 3 days from July 25, 1991, to April 1, 1992, and from December 23, 1993, to April 9, 1994; 168 days from April 10, 1994, to March 20, 1995; and 35 days at other times.
[5] German Space Agency
[6] Italian Space Agency
[7] During days 3–4 of the second mission, SIR-C/X was commanded to retrace the flight path of the first mission to acquire repeat-pass InSAR data with a 6-month time separation. From day 7 to the end of the second flight, the shuttle was commanded to repeat the flight path of the previous days to acquire 1-day, 2-day, and 3-day repeat-pass InSAR data.
[8] Japan Aerospace Exploration Agency
[9] Canadian Space Agency

in the Aleutian arc was at New Trident [Lu et al., 1997]. An ERS-1 interferogram indicated about 8 cm of uplift from 1993 to 1995 in an area about 2 km across, indicating a source about 1 km beneath the New Trident vent. Multiple InSAR images from 1995 to 2000 were processed to prospect for any additional deformation in the Katmai region. Plate 1b is an image averaged from five coherent interferograms that collectively span from 1995 to 2000. No significant (i.e., larger than 2–3 cm range change) large-scale deformation is indicated.

2.3. Peulik Volcano

Peulik Volcano (Plate 1c), a stratovolcano located on the Alaska Peninsula, is known to have erupted in 1814 and 1852 [Miller et al., 1998]. InSAR images that collectively span from July 1992 to August 2000 show that a deformation source located about 7 km beneath Peulik, presumably a magma body, inflated about 23 cm between October 1996 and September 1998. The average inflation rate was about 1.4 cm/month from October 1996 to September 1997 (Plate 1c); peaked at 2.3 cm/month between June 26, 1997, and October 9, 1997; and dropped to 0.5 cm/month from October 1997 to September 1998. Any deformation that occurred before October 1996 or after September 1998 was too small to be detected [Lu et al., 2002b]. An intense earthquake swarm occurred near Becharof Lake about 30 km northwest of Peulik from May to October 1998, around the end of the inflation period. Calculated static stress changes in the epicentral area due to the inflation beneath Peulik appear too small to provide a causal link, but the timing is suggestive nonetheless. The 1996–98 inflation episode at Peulik demonstrates that satellite InSAR can be used to detect magma accumulation beneath dormant volcanoes at least several months before other signs of volcanic or tectonic unrest are apparent.

2.4. Chiginagak Volcano

Chiginagak Volcano (Plate 1d) is a symmetric composite cone with a base about 8 km in diameter [Miller et al., 1998]. Snow and ice cover much of the uppermost part of the cone.

Historical eruptions occurred in 1929 and 1971. A fumarole issues from snow and ice on the northeast flank. Thick clouds of steam were observed issuing from this area in l997, 2000, and 2005. In October 1997, increased steaming, snowmelt, and sulfur smell were observed, and a thermal anomaly was registered on Advanced Very High Resolution Radiometer (AVHRR) satellite imagery. InSAR images acquired between 1992 and 2000, including a 1997–98 image that spans the 1997 eruption (Plate 1d), reveal no significant large-scale deformation.

2.5. Aniakchak Volcano

Aniakchak Caldera (Plate 1e) is 10 km in diameter, more than 1 km deep, and perennially ice-free. It formed by collapse about 3,430 years ago during the eruption of more than 50 km^3 of andesite-to-dacite magma [Miller et al., 1998]. Many dacitic eruptions have occurred since the caldera-forming event, most recently in May 1931, which suggests the presence of a large, silicic magma reservoir. InSAR images from 1992 through 2002 show that the floor of Aniakchak Caldera subsides about 13 mm/year (Plate 1e) [Kwoun et al., 2006]. The depth of the deformation source (~4 km) suggests that subsidence can be explained by the cooling or degassing of a shallow magma body and/or the reduction of pore-fluid pressure in a cooling hydrothermal system. Ongoing deformation of the volcano detected by InSAR, in combination with magmatic gas output from at least one warm spring and infrequent, low-level bursts of seismicity below the caldera, indicate that the magmatic system is still active.

2.6. Veniaminof Volcano

Mount Veniaminof (Plate 1f) is a broad central mountain, 35 km wide at the base, truncated by a spectacular steep-walled, ice-filled summit caldera about 10 km in diameter [Miller et al., 1998]. Glacier ice and perennial snow pack obscure much of the volcano's flanks. Frequent small eruptions, producing diffuse, ash-laden plumes, have been observed. Plate 1f shows an averaged InSAR image obtained by stacking multiple interferograms that collectively span from 1992 to 2000. Even though the image is not coherent in the summit area or upper flanks of the volcano due to snow and ice, any volcano-wide deformation can be ruled out.

2.7. Pavlof Volcano

Pavlof Volcano (Plate 1g) is approximately 7 km in base diameter and has active vents on the north and east sides, close to the summit [Miller et al., 1998]. Pavlof is the most active volcano in the Aleutian arc with almost 40 relatively well-documented eruptions dating back to 1790. Pavlof eruptions are typically strombolian to vulcanian in character and consist of the rhythmic ejection of incandescent bombs and ash. Recent vigorous eruptions occurred from 1986 to 1988 and from 1996 to 1997. The 1996–97 strombolian eruption produced lava fountains, lava flows, lahars, and ash plumes [Miller et al., 1998]. Examining InSAR images spanning intervals before, during, and after the 1996–97 eruption, we found no significant, volcano-wide deformation in areas where the images are coherent. Plate 1g shows an averaged interferogram comprising images that collectively span from 1992 to 2000; no significant deformation is apparent.

2.8. Dutton Volcano

Mount Dutton (Plate 1g) is a small calc-alkaline volcanic center with an approximate diameter of 5 km. The volcano consists of a central multiple-dome complex [Miller et al., 1998]. Although historical eruptions have not been reported, a swarm of shallow earthquakes (largest event $M_L = 4.0$) occurred beneath the volcano in July–August 1988. The seismic activity was interpreted as due to the fracturing of country rock as a dike intruded beneath Mount Dutton, which could be precursory to an eruption. Plate 1g shows an averaged interferogram that spans from 1992 to 2000. The image is coherent over most of the volcano, and any deformation is insignificant. However, Mount Dutton could have experienced an episode in 1988 similar to the one at Mount Peulik in 1996–98. In the latter case, deformation began two years before the Becharof Lake seismic swarm in 1998, but it did not persist after the swarm.

2.9. Shishaldin Volcano

Shishaldin Volcano (Plate 2a) is located near the center of Unimak Island in the eastern Aleutians. The spectacular symmetric cone has a base diameter of approximately 16 km and a small summit crater that typically emits a steam plume, occasionally with small amounts of ash. Shishaldin is the third most active volcano in the Aleutian arc, having erupted at least 28 times since 1775, including recent eruptions in 1995–96 and 1999. Multiple InSAR images, each spanning one year or more, show no significant deformation in coherent parts of the images before, during, or after the 1995–96 or 1999 eruptions (Plate 2a) [Moran et al., 2006]. This suggests that any pre-eruption inflation is compensated by subsequent withdrawal of a roughly equivalent volume of magma (resulting in no net deformation), which in turn suggests that magma accumulation and transport occur relatively quickly.

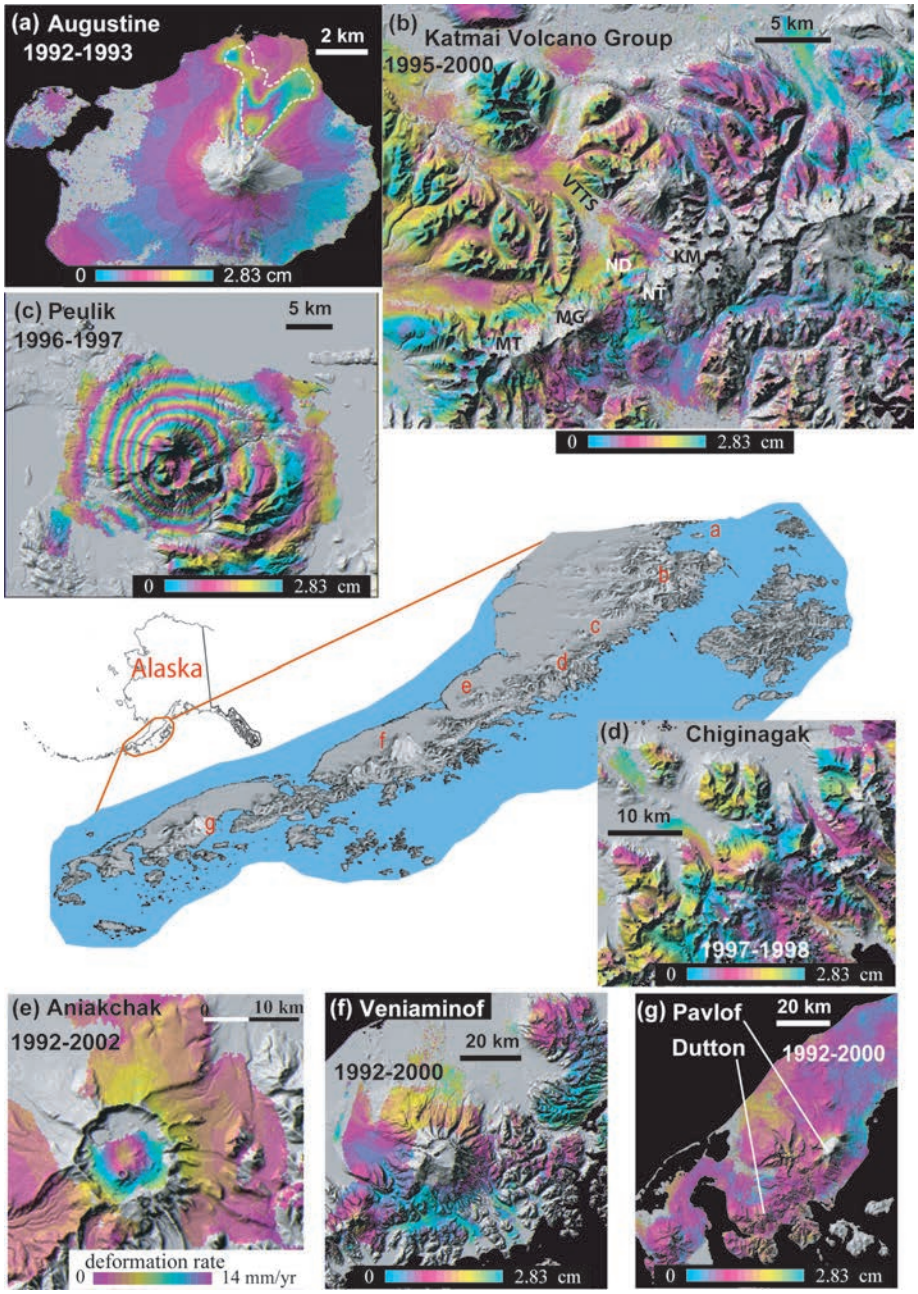

Plate 1. InSAR images for volcanoes in the eastern segment of the Aleutian arc. (a) InSAR image of Augustine volcano (1992-1993), depicting deformation associated with compaction of the 1986 pyroclastic flow deposits outlined by the white dashed line. (b) Averaged interferogram for the Katmai volcano group, showing no significant deformation during 1995-2000. VTTS – Valley of Ten Thousand Smokes; ND – Novarupta Dome; KT – Katmai caldera; NT – New Trident; MG – Mageik; MT – Martin. (c) InSAR image of Peulik volcano showing ~17 cm of uplift centered on the volcano's southwest flank from October 1996 to October 1997. (d) InSAR image (1997-1998) bracketing the October 1997 eruption of Chiginagak volcano, showing no significant deformation associated with the eruption. Localized subsidence (dashed line) was most likely caused by outgassing from an active fumarole. (e) Averaged InSAR image of Aniakchak Volcano showing that the caldera subsided about 13 mm/yr from 1992 to 2002. (f) Averaged interferogram of Veniaminof volcano, showing no significant deformation during 1992-2000. (g) Averaged interferogram (1992-2000) for Pavlof and Dutton volcanoes, showing no detectable deformation. Each interferometric fringe (full color cycle) represents 2.83 cm of range change between the ground and the satellite unless otherwise noted. The color change from red to yellow, blue, and red in a fringe represents a relative increase in satellite-to-ground distance or an away-from-satellite ground motion. Interferograms are draped over DEM shaded relief images. Areas without interferometric coherence are gray.

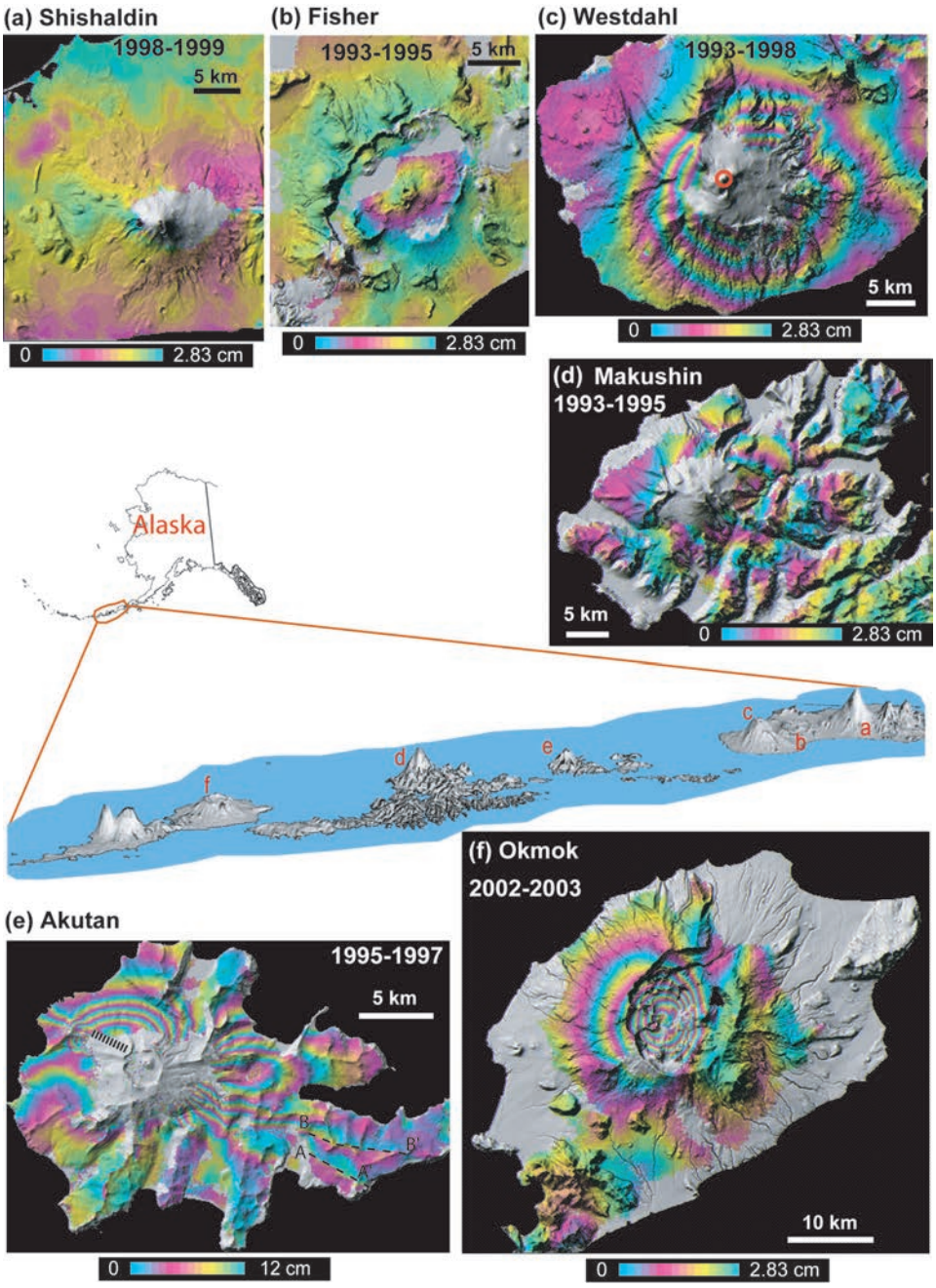

Plate 2. InSAR images for volcanoes in the central segment of the Aleutian arc. (a) InSAR image (1998–1999) of Shishaldin Volcano that shows no significant deformation associated with the volcano's 1999 eruption. (b) InSAR image of Fisher volcano, showing volcano-wide subsidence during 1993–1995. (c) Aseismic inflation of Westdahl volcano depicted by a 1993–1998 InSAR image. Circle marks the surface projection of a shallow magma reservoir beneath Westdahl Peak. (d) A 1993-1995 interferogram of Makushin volcano, showing about 7 cm inflation associated with a likely eruption in January 1995. (e) L-band JERS-1 InSAR image showing the complex deformation field at Akutan Volcano that accompanied an intense earthquake swarm in March 1996. Thick dashed line represents a zone of ground cracks that formed during the swarm. Dashed lines (A-A' and B-B') represent normal faults that were reactivated. (f) Deformation interferogram of Okmok volcano, showing inflation of about 20 cm during 2002–2003. Each interferometric fringe (full color cycle) represents 2.83 cm of range change between the ground and the satellite unless otherwise noted. The color change from red to yellow, blue, and red in a fringe represents a relative increase in satellite-to-ground distance or an away-from-satellite ground motion. Interferograms are draped over DEM shaded relief images. Areas without interferometric coherence are gray.

2.10. Fisher Volcano

Fisher Caldera (Plate 2b) is 11 km wide, 18 km long, and filled with active fumaroles. It formed about 9,000 years ago and is one of the largest calderas in the Aleutian arc. Its last significant eruption occurred in the 1820s, but hydrothermal activity remains strong. Multiple interferograms spanning from 1992 to 2000 indicate that the volcano has been subsiding. Plate 2b shows the result for 1993–95: a maximum of about 3 cm of volcano-wide subsidence. This observation is consistent with GPS measurements in the area [Mann and Freymueller, 2003]. Subsidence is most likely due to depressurization of the vigorous hydrothermal system beneath Fisher Caldera.

2.11. Westdahl Volcano

Westdahl Volcano, a young glacier-clad shield volcano, was frequently active during the latter half of the 20th century with documented eruptions in 1964, 1978–79, and 1991–92 [Miller et al., 1998; Lu et al., 2004]. The background level of seismic activity since the last eruption was generally low (about five $M < 3$ earthquakes per year). InSAR images from 1991 to 2000 show that Westdahl Volcano deflated during its 1991–92 eruption and is re-inflating at a rate that could produce another eruption in the near future (Plate 2c). The images suggest that rates of post-eruptive inflation and co-eruptive deflation are approximated by exponential decay functions with time constants of about six years and a few days, respectively [Lu et al., 2000b, 2003b]. This behavior is consistent with a deep, constant-pressure magma source connected to a shallow reservoir (about 6 km below sea level) by a magma-filled conduit. The magma flow rate is governed by the pressure gradient between the deep source and the shallow reservoir [Lu et al., 2003b].

2.12. Makushin Volcano

Makushin Volcano (Plate 2d), a broad, ice-capped, truncated stratovolcano, is one of the more active volcanoes in the Aleutians, having produced at least 17 relatively small explosive eruptions since the late 1700s [Miller et al., 1998]. Additional smaller eruptions probably occurred during this period but were unrecorded, either because they occurred when the volcano was obscured by clouds or because the eruptive products did not extend beyond the volcano's flanks. Several independent InSAR images, each spanning the time period from October 1993 to September 1995, show evidence of about 7 cm of uplift (Plate 2d) centered on the volcano's east flank. The uplift was interpreted as pre-eruptive inflation associated with a small, poorly documented explosive eruption on January 30, 1995 [Lu et al., 2002c].

2.13. Akutan Volcano

Akutan Volcano (Plate 2e), the second most active volcano in Alaska [Miller et al., 1998], was shaken in March 1996 by an intense earthquake swarm accompanied by extensive ground cracking but no eruption. InSAR images from both the L-band Japanese Earth Resources Satellite (JERS)-1 (Table 1) and C-band ERS-1/ERS-2 (Table 1) show uplift by as much as 60 cm on the western part of the island associated with the swarm. The L-band JERS-1 interferogram (Plate 2e) displays greater coherence, especially in areas with loose surface material or thick vegetation where C-band interferograms lose coherence. The JERS-1 interferogram also shows subsidence of a similar magnitude on the eastern part of the island, as well as displacements along faults (A–A' and B–B' in Plate 2e) that were reactivated during the seismic swarm [Lu et al., 2000a, 2005b]. The axis of uplift and subsidence strikes about N70°W and is roughly parallel to 1) a zone of fresh cracks on the volcano's northwest flank, 2) normal faults that cut the island, and 3) the inferred maximum compressive stress direction. Multiple InSAR images spanning time intervals both before and after the swarm suggest that the northwest flank was uplifted 5–20 mm/year relative to the southwest flank, probably by magma intrusion [Lu et al., 2005b].

2.14. Okmok Volcano

Okmok Volcano (Plate 2f), a broad shield topped with a 10-km-wide caldera, produced blocky, basaltic lava flows during relatively large effusive eruptions in 1945, 1958, and 1997 [Miller et al., 1998]. Multiple InSAR images reveal 1) surface inflation of more than 18 cm from 1992 to 1995 and subsidence of 1–2 cm from 1995 to 1996, prior to the 1997 eruption; 2) more than 140 cm of surface deflation during the 1997 eruption; and 3) 5–15 cm/year inflation from 1997 to 2004, after the 1997 eruption [Lu et al., 1998, 2000c, 2003c, 2005a; Mann et al., 2002]. Plate 2f is a Radarsat-1 (Table 1) InSAR image that depicts about 20 cm of inflation from 2002 to 2003. Numerical modeling suggests that the magma reservoir responsible for the deformation is located about 3 km beneath the center of the caldera and about 5 km northeast of the 1997 eruptive vent [Mann et al., 2002; Lu et al., 2005a].

2.15. Cleveland Volcano

Cleveland Volcano (Figs. 3a and 3b), a stratovolcano in the central-western Aleutian arc, is frequently observed emitting steam and ash. Most of the activity is characterized as profuse steaming from the summit crater with intermittent emissions of ash and occasional debris flows. Recent explosive eruptions occurred in February–April 2001 and

July 2005 (www.avo.alaska.edu). Multiple interferograms before, during, and after the 2001 and 2005 eruptions do not reveal any significant volcano-wide deformation. Plates 3a and 3b show two interferograms spanning the 2001 and 2005 eruptions, respectively.

2.16. Korovin Volcano

Korovin Volcano (Plate 3c) is a stratovolcano on Atka Island in the central Aleutian arc. It has a basal diameter of 7 km and two summit vents 0.6 km apart. Intercalated lava flows and pyroclastic rocks make up the volcano. Korovin erupted in 1951, 1953–54, 1973, 1976, 1986–87, and 1998. An interferogram spanning the 1998 eruption is shown in Plate 3c. It indicates that deformation associated with the eruption is either lacking or too small to be detected by ERS-1/ERS-2 (Table 1) InSAR.

2.17. Kiska Volcano

Kiska Volcano (Plate 3d) is the westernmost historically active volcano in the Aleutian arc. Sequential InSAR images show a circular area about 3 km in diameter centered near the summit that subsided as much as 10 cm from 1995 to 2001, mostly during 1999–2000 (Plate 3d). Based on the shallow source depth from modeling (< 1 km), the copious amounts of steam that were vented during recent eruptions, and recent field reports of vigorous steaming and persistent ground shaking near the summit area, the observed subsidence is attributed to decreased pore-fluid pressure in a shallow hydrothermal system beneath the summit area [Lu et al., 2002a].

2.18. Seguam Volcano

Seguam Island (Plate 3e) consists of two late Quaternary calderas. The western caldera dominates the western half of the island and includes Pyre Peak (commonly referred to as Seguam Volcano), a 3-km-wide central cone. Historical eruptions occurred in 1901, 1927, and 1977, mostly from vents at or near Pyre Peak. The historically inactive eastern caldera is somewhat larger than its western counterpart and contains a central cone and several vents. In late December 1992 a small satellite cone a few km southwest of Pyre Peak erupted, sending an ash plume to 1,200 m. Intermittent explosive eruptions were reported from May 28, 1993, to August 19, 1993. InSAR images spanning various intervals from 1992 to 2000 document co-eruptive and post-eruptive deformation (Figs. 3e–3g). Interferograms that span the 1992–93 eruption are characterized by a relatively broad pattern of uplift that is roughly centered on the eastern (historically inactive) caldera and elongated along the long axis of Seguam Island. Deformation during the first few years following the eruption was dominated by two separate regions of subsidence, each having radial symmetry roughly centered on the east and west calderas, respectively. During the later post-eruption intervals, the pattern of deformation in the eastern caldera changed from subsidence to broad uplift. A model that combines magma influx, thermoelastic relaxation, and poroelastic effects accounts for the observed deformation [Lu et al., 2003a; Masterlark and Lu, 2004; Price, 2004].

3. SUMMARY

The satellite InSAR technique has proven to be a powerful space-borne geodetic tool for studying a variety of volcanic processes by analyzing surface deformation patterns along the Aleutian arc [Lu et al., 1997, 1998, 2000a–c, 2002a–c, 2003a–c, 2004, 2005 a–b] and at other volcanoes worldwide [e.g., Amelung et al., 2000; Massonnet et al., 1995; Pritchard and Simons, 2004; Rosen et al., 1996; Zebker et al., 2000; Sturkell et al., 2006; Wicks et al., 1998, 2002]. InSAR's all-weather, large-area imaging capability makes it particularly useful in this regard.

InSAR is an excellent technique for detecting subtle deformation of the ground surface, which can be used to identify restless volcanoes long before seismic or other precursory signals are detected. This is well illustrated by InSAR results for Westdahl and Mount Peulik Volcanoes. Each has a magma reservoir ~6–7 km deep, which is below the brittle-ductile transition that typically occurs ~5 km beneath volcanoes [Sibson, 1982]. Therefore, the slow ascent of magma to the reservoirs generally is not marked by earthquakes. The 1996–98 inflation episode at Mount Peulik most likely would have gone undetected if not for the occurrence of the Becharof Lake earthquake swarm, which was the impetus for the InSAR study of the area [Lu et al., 2002b]. Even though the 1996–98 epicenters are not well constrained, it is clear that most of the activity occurred 20–45 km northwest of Mount Peulik, and few if any earthquakes occurred within 10 km of the volcano. We suspect that such episodes are relatively common and an integral part of the eruption cycle for volcanoes with characteristically long repose periods [e.g., Wicks et al., 2002]. Many of these episodes occur aseismically because magma accumulates gradually and preferentially near the brittle-ductile transition in the crust. In such cases, inflation episodes will likely go undetected unless the intrusion rate is high enough to cause brittle failure or the regional stress field is such that a small amount of incremental stress is sufficient to trigger earthquakes along favorably oriented faults at some distance from the volcano. In light of the Mount Peulik results, we suspect that the eruption cycle

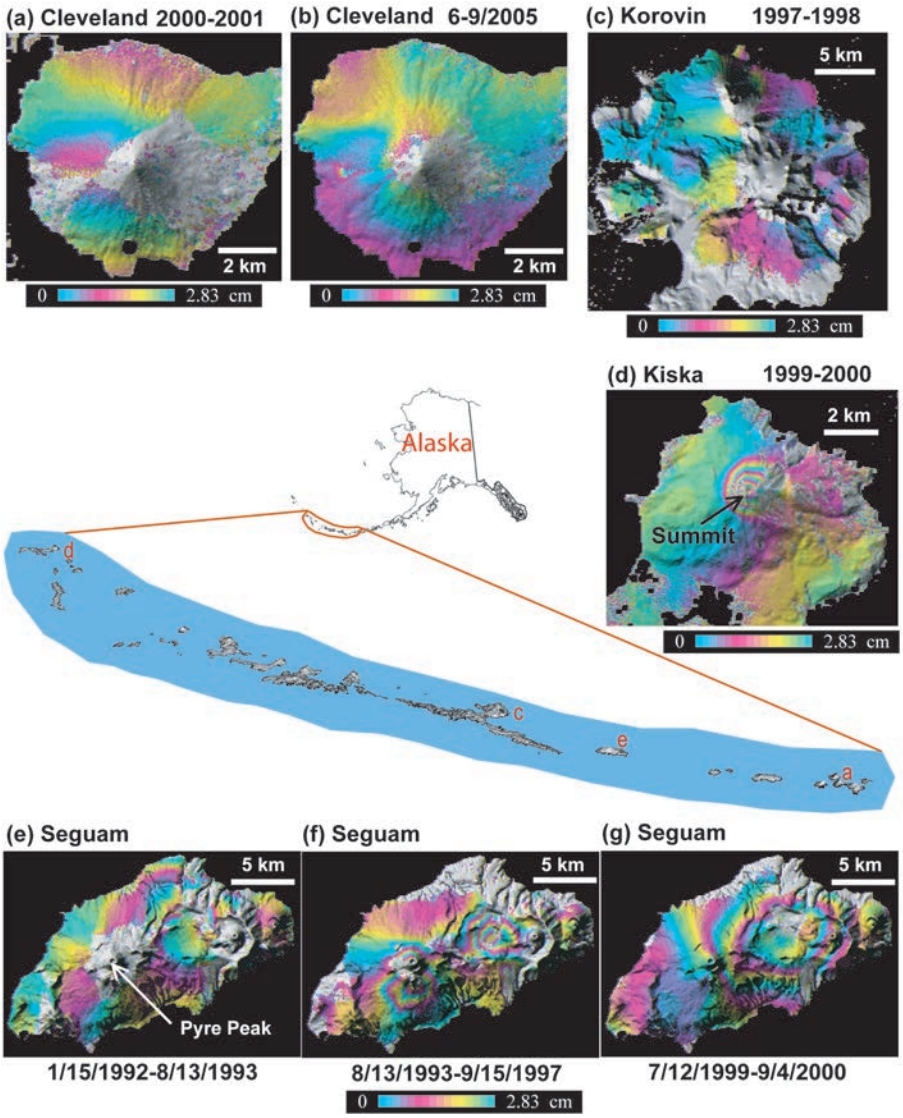

Plate 3. InSAR images for volcanoes in the western segment of the Aleutian arc. (a) InSAR image (2000–2001) of Cleveland volcano that shows no significant deformation associated with the volcano's 2001 eruption. (b) InSAR image (June-September 2005) of Cleveland volcano that shows no significant deformation associated with the volcano's July 2005 eruption. (c)InSAR image (1997-1998) of Korovin volcano, showing no significant deformation associated with the 1998 eruption. (d) InSAR image of Kiska volcano (August 1999-August 2000), showing subsidence of the summit related to hydrothermal activity. (e) InSAR image (January 15-August 13, 1993) of Seguam, showing deformation associated with the 1993 eruption. (f) InSAR image (1993-1997) of Seguam, showing deformation in the first few years after the 1993 eruption. (g) InSAR image of Seguam, showing deformation during 1999-2000, 6-7 years after the 1993 eruption. Each interferometric fringe (full color cycle) represents 2.83 cm of range change between the ground and the satellite. The color change from red to yellow, blue, and red in a fringe represents a relative increase in satellite-to-ground distance or an away-from-satellite ground motion. Interferograms are draped over DEM shaded relief images. Areas without interferometric coherence are gray.

at other dormant stratovolcanoes is much more eventful than has been recognized previously. Such volcanoes might inflate episodically during long periods of apparent quiescence until some threshold is reached, triggering magma's final ascent to the surface. If so, InSAR provides a valuable tool for tracking a volcano's progress from one eruption to the next and for identifying quiescent volcanoes that warrant careful monitoring.

InSAR can image deformation over a large region, which makes it an attractive tool for studying a complex deformation field such as the one that accompanied the 1996 seismic swarm at Akutan Volcano. To adequately characterize such a complex deformation field using a more conventional geodetic technique (e.g., electronic distance measurement (EDM), tiltmeters, strainmeters, or even GPS) would require measurements at a very large number of benchmarks or instrument stations. For remote volcanoes such as those in the Aleutian arc, the resulting workload would be prohibitive. A conventional geodetic network would have to be extensive enough to capture the entire deformation field at each potentially active volcano, as well as dense enough to adequately characterize possible small-scale complexities. InSAR overcomes this limitation of conventional geodesy, at least in areas of adequate radar coherence, by providing a more spatially complete image of the deformation field. In the future, combining areal measurements from InSAR with three-dimensional measurements from GPS will almost surely advance our understanding of the dynamics of magmatic processes.

Based on deformation patterns observed with InSAR at about 20 Aleutian volcanoes, we can make the following statements:

1. Deformation patterns at Aleutian volcanoes are diverse. This probably reflects the fact that Aleutian volcanoes span a broad spectrum of eruptive styles, sizes, magma compositions, and local tectonic settings. Differing deformation patterns suggest differences in the magma plumbing systems as well. For example, Unimak Island hosts three active volcanoes: Westdahl, Fisher, and Shishaldin. In terms of eruption frequency, Shishaldin is the most active among the group, and Fisher is the least active. Our InSAR analysis suggests that Westdahl is persistently inflating at a rate that declined since the last eruption in 1991–92 and that there is a magma reservoir ~6 km below the sea level beneath Westdahl Peak (circle in Plate 2c). Because Shishaldin is more active than Westdahl, one might expect more deformation at Shishaldin. However, InSAR shows that, on the contrary, significant deformation was lacking before, during, and after the 1995–96 and 1999 eruptions at Shishaldin [Moran et al., 2006]. Deformation at Fisher differs from that observed at either Westdahl or Shishaldin: Fisher is subsiding at a rate of 1–2 cm/year. Even though these three volcanoes are only 10–20 km apart, their deformation behaviors are remarkably different.
2. The more frequently active volcanoes, such as Shishaldin, Pavlof, and Cleveland, exhibit little or no measurable deformation. All of these three volcanoes are stratovolcanoes, have symmetric cones, and erupt frequently. Interferograms that span time intervals before, during, and after recent eruptions do not show any significant deformation. Plausible explanations include the following: 1) pre-eruptive inflation is balanced by co-eruptive deflation, resulting in little or no net deformation; 2) the magma reservoirs are deep, so inflation or deflation causes only broad, subtle deformation of the surface that is difficult to detect, especially if the area of radar coherence is limited [Moran et al., 2006]; 3) no significant pre-eruptive and co-eruptive deformation is associated with these eruptions; and 4) the magma reservoir is very shallow and its strength is small (i.e., pressure or volume changes in the reservoir are small), so deformation only occurs over a small area (a few km in radius) near the summit where coherence is lost owing to perennial ice or snow. The third possibility is puzzling, because considerable deformation has been observed with InSAR in association with similar-sized eruptions and intrusions at other Aleutian volcanoes. Considering the size of recent eruptions at these volcanoes, the last alternative also seems unlikely [Moran et al., 2006]. If pre-eruption inflation were compensated by subsequent withdrawal of a roughly equivalent volume of magma (resulting in no net deformation, alternative 1), the InSAR studies suggest that magma transport and accumulation occur relatively quickly. Further study requires better temporal sampling than is available from current SAR satellites and an L-band sensor to defeat interferometric decorrelation due to snow/ice cover. Better monitoring of this type of volcano also requires observations from continuous GPS and seismometers to capture localized or short-term deformation, if it exists.
3. Through numerical modeling, InSAR-derived images can be used to infer sources that cause observed deformation. However, modeling cannot uniquely characterize the source(s), for at least two reasons. First, numerical inversion solutions are inherently non-unique, i.e., any deformation field can be modeled equally well by different sets of superimposed sources. Only by limiting the solution to a single source, or a small number of sources, can we make inferences about the cause of observed deformation (e.g., magmatic or hydrothermal, or in the first case, sphere, ellipsoid, dike, or sill). A second reason that numerical models are non-unique is that volcanic deformation can be caused by changes in either mass or pressure, in either the

magmatic or hydrothermal system. For example, magma can be added to a reservoir from below or withdrawn to feed an intrusion or eruption. Alternatively, exsolution of volatiles during cooling and crystallization of reservoir magma can increase reservoir pressure with no change in mass, and subsequent escape of exsolved volatiles can depressurize the reservoir with negligible mass change [Dzurisin, 2007]. In the latter case, ground uplift might be observed if fluids released from cooling magma are trapped underground at lithostatic pressure, but subsidence can be expected when fluids escape into the hydrostatically pressured part of the system [Fournier, 2007]. At large calderas in particular, numerical simulations have suggested hydrothermal fluid flow can produce significant ground surface deformation [Hurwitz et al., 2007].

4. For the deforming Aleutian volcanoes discussed in this paper, we attribute most of the observed uplifts (e.g., Westdahl, Peulik, and Makushin) to magma intrusion, in large part because the model sources are located at 5-7 km depth. This is deeper than hydrothermal fluids are thought to exist in active volcanic environments [Fournier, 2007]. On the other hand, we interpret persistent subsidence at Kiska volcano as being due to fluid loss from the hydrothermal system, mainly for two reasons: (1) the model deformation source is only about 1 km deep, and (2) steam emissions are commonly observed at the volcano [Lu et al., 2002a]. For the reasons discussed above, we realize that a deep model source is not synonymous with magma, nor is a shallow source at a steaming volcano compelling evidence for a hydrothermal deformation mechanism. In the absence of additional information from microgravity measurements, fluid geochemistry, or scientific drilling, any conclusion about the source(s) of ground deformation is necessarily reduced to a plausibility argument. We believe that magmatic, hydrothermal, and tectonic sources all play a role in causing the surface deformation observed at Aleutian volcanoes. In specific cases, one of these mechanisms is likely to be dominant. We have tried here to identify those mechanisms for a few of the Aleutian volcanoes, recognizing that the available data are inherently ambiguous. Because magma is denser than hydrothermal fluid, high-precision gravity surveys in conjunction with surface deformation and groundwater measurements can help to resolve this ambiguity in some cases [Gottsmann and Rymer, 2002].
5. For some of the Aleutian volcanoes including Okmok, Akutan, Seguam, and Westdahl, InSAR deformation mapping was conducted intensively using SAR images from all of the available sensors (ERS-1, ERS-2, JERS-1, Radarsat-1, and Envisat) (Table 1). For these volcanoes, multi-temporal InSAR images enable construction of virtual magma plumbing systems that can be used to constrain models of magma accumulation and to help anticipate future eruptions. For other volcanoes, including Chiginagak, Veniaminof, and Korovin, InSAR results are still quite preliminary and comprehensive analyses are yet to be completed. Nonetheless, results presented in this paper can serve as a basis for more thorough analyses in the future.

Our studies suggest that some Aleutian volcanoes are much more active, in terms of magma movement as indicated by surface deformation from InSAR, during repose periods than reliance solely on seismic signals might suggest. That is not to say that InSAR is the final piece in a puzzle that has occupied volcanologists for decades. In fact, we are far from a complete understanding of the eruption cycle at most of Earth's highly diverse volcanoes includes those summarized in this paper. As a result, the discovery of ground deformation (or lack thereof) at a given volcano using InSAR or any other geodetic technique does not necessarily result in better allocation of monitoring resources or more informed assessments of volcano hazards. We know that some volcanoes erupt without deforming and others deform without erupting. Likewise, some eruptions are preceded or accompanied by intense seismic activity or copious releases of magmatic gases, while others are not. The challenge in the Aleutians and elsewhere is to better understand why this is the case. For that endeavor, more and better information about how volcanoes deform is surely an advantage—and InSAR is an important new source of such information.

With more operational SAR sensors available for rapid and frequent data acquisitions, future InSAR will escort volcano monitoring to an important phase wherein magma accumulation in the middle to upper crust can be observed long before the onset of short-term precursors to an eruption. Ultimately, more widespread use of InSAR for volcano monitoring could shed light on a poorly understood but important part of the eruption cycle, i.e., the time period between eruptions when a volcano seems to be doing essentially nothing. This potential makes InSAR a promising space-based, long-term volcano monitoring tool. Combining applications of the InSAR technique with observations from continuous GPS, gravimeters, strainmeters, tiltmeters, seismometers, and volcanic gas sensors will surely improve our capability to forecast future eruptions, thus enabling improved volcano hazard assessment and more effective eruption preparedness.

Acknowledgments. ERS-1, ERS-2, Envisat, Radarsat-1, and JERS-1 SAR images are copyrighted © 1991–2005 European Space Agency (ESA), Canadian Space Agency (CSA), and Japan Aerospace Exploration Agency (JAXA), respectively, and were provided by Alaska Satellite Facility (ASF), ESA, and JAXA.

The research summarized in the paper was supported by funding from the NASA Radarsat Program, NASA Solid Earth & Natural Hazards Program, USGS Volcano Hazards Program, USGS Land Remote Sensing Program, and USGS contract O3CRCN0001. We thank ASF, JAXA, and ESA staff members for their special efforts in making SAR data available to us on a timely basis. We also thank J. Freymueller, D. Mann, T, Masterlark, V. McConnell, D. Meyer, S. Moran, W. Thatcher, T. Neal, and many other colleagues for contributions to this research. Constructive comments and edits by J. Eichelberger, P. Lundgren, B. Penga, D. Steinwand, and P. Burns were greatly appreciated.

REFERENCES

Amelung, F., S. Jonsson, H. Zebker, and P. Segall (2000), Widespread uplift and 'trapdoor' faulting on Galapagos volcanoes observed with radar interferometry, *Nature*, *407*, 993–996.

Cervelli, P., M. H. Murray, P. Segall, Y. Aoki, and T. Kato (2001), Estimating source parameters from deformation data, with an application to the March 1997 earthquake swarm of the Izu Peninsula, Japan, *J. Geophys. Res.*, *106* , 11,217–11,237.

Davis, P. M. (1986), Surface deformation due to inflation of an arbitrarily oriented triaxial ellipsoidal cavity in an elastic half-space, with reference to Kilauea Volcano, Hawaii, *J. Geophys. Res.*, *91*, 7429–7438.

Dvorak, J., and D. Dzurisin (1997), Volcano geodesy: The search for magma reservoirs and the formation of eruptive vents, *Rev. Geophys.*, *35*, 343–384.

Dzurisin, D. (2007), *Volcano Deformation – Geodetic Monitoring Techniques*, 441 pp., Springer-Praxis Publishing Ltd, Chichester, UK.

Dzurisin, D. (2003), A comprehensive approach to monitoring volcano deformation as a window on eruption cycle, *Rev. Geophys., Review of Geophysics*, *41*, 10.1029/2001RG000107.

Fialko, Y., Y. Khazan, and M. Simons (2001), Deformation due to a pressurized horizontal circular crack in an elastic half-space, with applications to volcano geodesy, *Geophys. J. Int.*, *146*, 181–190.

Fournier, R. (2007), Hydrothermal system and volcano geochemistry, in *Volcano Deformation—Geodetic Monitoring Techniques*, by D. Dzurisin, 323–342, Springer-Praxis Publishing Ltd, Chichester, UK.

Gottsmann, J., and H. Rymer (2002), Deflation during caldera unrest: Constraints on subsurface processes and hazard prediction from gravity-height data, *Bull. Volcanol.*, *64*, 338–348.

Hildreth, W. (1983), The compositionally zoned eruption of 1912 in the Valley of Ten Thousand Smokes, Katmai National Park, Alaska: *Journal of Volcanology and Geothermal Research*, *18*, 1–56.

Hurwitz, S., L. Christiansen, and P. Hsieh (2007), Hydrothermal fluid flow and deformation in large calderas: Inferences from numerical simulations, *J. Geophys. Res.*, *112*, B02206, doi:10.1029/2006JB004689.

Kwoun, O., Z. Lu, C. Neal, and C. Wicks (2006), Quiescent deformation of the Aniakchak Caldera, Alaska, mapped by InSAR, *Geology*, *34*, 5–8.

Lu, Z., T. Masterlark, and D. Dzurisin (2005a), Interferometric Synthetic Aperture Radar (InSAR) Study of Okmok Volcano, Alaska, 1992–2003: Magma Supply Dynamics and Post-emplacement Lava Flow Deformation, *Journal of Geophysical Research*, *110*, B02403, DOI:10.1029/2004JB003148.

Lu, Z., C. Wicks, O. Kwoun, J. Power, and D. Dzurisin (2005b), Surface deformation associated with the March 1996 earthquake swarm at Akutan Island, Alaska, revealed by C-band ERS and L-band JERS radar interferometry, *Canadian Journal of Remote Sensing*, *31*, 7–20.

Lu, Z., R. Rykhus, T. Masterlark, and K. Dean (2004), Mapping recent lava flows at Westdahl volcano, Alaska, using radar and optical satellite imagery, *Remote Sensing of Environment*, *91*, 345–353.

Lu, Z., C. Wicks, D. Dzurisin, J. Power, W. Thatcher, and T. Masterlark (2003a), Interferometric synthetic aperture radar studies of Alaska volcanoes, *Earth Observation Magazine (EOM)*, *12* (3), 8–18.

Lu, Z., T. Masterlark, D. Dzurisin, R. Rykhus, and C. Wicks (2003b), Magma Supply Dynamics at Westdahl Volcano, Alaska, Modeled from Satellite Radar Interferometry, *Journal of Geophysical Research*, *108*, 2354, 10.1029/2002JB002311.

Lu, Z., E. Fielding, M. Patrick, and C. Trautwein (2003c), Estimating Lava Volume by Precision Combination of Multiple Baseline Spaceborne and Airborne Interferometric Synthetic Aperture Radar: the 1997 Eruption of Okmok Volcano, Alaska, *IEEE Transactions on Geoscience and Remote Sensing*, *41*, 1428–1436.

Lu, Z., T. Masterlark, J. Power, D. Dzurisin, and C. Wicks (2002a), Subsidence at Kiska volcano, Western Aleutians, Detected by Satellite Radar Interferometry, *Geophysical Research Letters*, *29*, 1855, doi:10.1029/2002GL014948.

Lu, Z., C. Wicks, D. Dzurisin J. Power, S. Moran, and W. Thatcher (2002b), Magmatic Inflation at a Dormant Stratovolcano: 1996–98 Activity at Mount Peulik Volcano, Alaska, Revealed by Satellite Radar Interferometry, *Journal of Geophysical Research*, *107*, 2134, doi:10.1029/2001JB000471.

Lu, Z., J. Power, V. McConnell, C. Wicks, and D. Dzurisin (2002c), Pre-Eruptive Inflation and Surface Interferometric Coherence Characteristics Revealed by Satellite Radar Interferometry at Makushin Volcano, Alaska: 1993–2000, *Journal of Geophysical Research*, *107*, 2266, doi:10.1029/2001JB000970.

Lu, Z., C. Wicks, J. Power, and D. Dzurisin (2000a), Ground deformation associated with the March 1996 earthquake swarm at Akutan volcano, Alaska, revealed by satellite radar interferometry, *Journal of Geophysical Research*, *105*, 483–21,496.

Lu, Z., C. Wicks, D. Dzurisin, W. Thatcher, J. Freymueller, S. McNutt, and D. Mann (2000b), Aseismic inflation of Westdahl volcano, Alaska, revealed by satellite radar interferometry, *Geophysical Research Letters*, *27*, 1567–1570.

Lu, Z., D. Mann, J. Freymueller, and D. Meyer (2000c), Synthetic aperture radar interferometry of Okmok volcano, Alaska: Radar observations, *Journal of Geophysical Research*, *105*, 10791–10806.

Lu, Z., D. Mann, and J. Freymueller (1998), Satellite radar interferometry measures deformation at Okmok volcano, *EOS Transactions*, *79*, 461–468.

Lu, Z., and J. Freymueller (1998), Synthetic aperture radar interferometry coherence analysis over Katmai volcano group, Alaska, *Journal of Geophysical Research*, *103*, 29887–29894.

Lu, Z., R. Fatland, M. Wyss, S. Li, J. Eichelberger, K. Dean, and J. Freymueller (1997), Deformation of New Trident volcano measured by ERS-1 SAR interferometry, Katmai national Park, Alaska, *Geophys. Res. Lett*., *24*, 695–698.

Mann, D., and J. Freymueller (2003), Volcanic and tectonic deformation on Unimak Island in the Aleutian Arc, Alaska, *J. Geophys. Res*., *108*, 2108, doi:10.1029/2002JB001925.

Mann, D., J. Freymueller, and Z. Lu (2002), Deformation associated with the 1997 eruption of Okmok volcano, Alaska, *J. Geophys. Res*., *107*, 10.1029/2001JB000163.

Massonnet, D., P. Briole, and A. Arnaud (1995), Deflation of Mount Etna monitored by spaceborne radar interferometry, *Nature*, *375*, 567–570.

Massonnet, D., and K. Feigl (1998), Radar interferometry and its application to changes in the Earth's surface, *Rev. Geophys*., *36*, 441–500.

Masterlark, T., and Z. Lu (2004), Transient volcano deformation sources imaged with InSAR: Application to Seguam island, Journal of Geophysical Research, *J. Geophys. Res. 109*, B01401, doi:10.1029/2003JB002568.

Masterlark, T., Z. Lu, and R. Rykhus (2006), Thickness distribution of a cooling pyroclastic flow deposit: Optimization using InSAR, FEMs, and an adaptive mesh algorithm, *Journal of Volcanology and Geothermal Research*, *150*, 186–201.

Miller, T.M., R.G. McGimsey, D.H. Richter, J.R. Riehle, C.J. Nye, M.E. Yount, and J.A. Dumoulin (1998), Catalog of the historically active volcanoes of Alaska, *USGS Open-File Report*, *98-582*, 1998.

Mogi, K. (1958), Relations between the eruptions of various volcanoes and the deformations of the ground surface around them, *Bull. Earthquake Res. Inst. Univ. Tokyo*, *36*, 99–134.

Moran, S., O. Kwoun, T. Masterlark, and Z. Lu (2006), On the absence of deformation signals from InSAR interferograms bracketing the 1995–1996 and 1999 eruptions of Shishaldin Volcano, Alaska, *Journal of Volcanology and Geothermal Research*, *150*, 119–131.

Okada, Y. (1985), Surface deformation due to shear and tensile faults in a half-space, *Bull. Seismol. Soc. Am*., *75*, 1135–1154.

Price, E. (2004), Dynamic deformation of Seguam Island, Aleutian Islands, Alaska, 1993–2000: Implications for magmatic and hydrothermal processes, *J. Geophys. Res*., *109*, 10.1029/2003JB002671.

Pritchard, M., and M. Simons (2004), Surveying volcanic arcs with satellite radar interferometry: The central Andes, Kamchatka, and beyond, *Geological Society of America (GSA) Today*, *14*, 4–11.

Rosen, P., S. Hensley, H. Zebker, F. H. Webb, and E. J. Fielding (1996), Surface deformation and coherence measurements of Kilauea volcano, Hawaii, from SIR-C radar interferometry, *J. Geophys. Res*., *101*, 23109–23125.

Sibson, R. (1982), Fault zone models, heat flow, and the depth distribution of seismicity in the continental crust of the United States, *Bull. Seismol. Soc. Am*., *72*, 151–163.

Sturkell, E. and others (2006), Volcano geodesy and magma dynamics in Iceland, *Journal of Volcanology and Geothermal Research*, *150*, 14–34.

Wicks, C., W. Thatcher, and D. Dzurisin (1998), Migration of fluids beneath Yellowstone Caldera inferred from satellite radar interferometry, *Science*, *282*, 458–462.

Wicks, C.W. Jr., Dzurisin, D., Ingebritsen, S., Thatcher, W., Lu, Z., and Iverson, J. (2002), Magmatic activity beneath the quiescent Three Sisters volcanic center, central Oregon Cascade Range, USA, *Geophys. Res. Lett*., *29*, doi: 10.1029/2001GL014205.

Yang, X.-M., P. M. Davis, and J. H. Dieterich (1988), Deformation from inflation of a dipping finite prolate spheroid in an elastic half-space as a model for volcanic stressing, *J. Geophys. Res*., *93*, 4249–4257, 1988.

Zebker, H., F. Amelung, and S. Jonsson (2000), Remote sensing of volcano surface and internal processing using radar interferometry, *Remote Sensing of Active Volcanism*, AGU Monograph, edited by P. Mouginis-Mark et al., 179–205.